Pal and Ghosh *Journal of Theoretical and Applied Physics* 2012, **6**:42
http://www.jtaphys.com/content/6/1/42

Journal of Theoretical and Applied Physics
a SpringerOpen Journal

RESEARCH Open Access

Influence of periodically propagating impurity and accompanying time variation of impurity spread on excitation profile of doped quantum dots

Suvajit Pal[1] and Manas Ghosh[2*]

Abstract

We investigate the excitation behavior of a repulsive impurity-doped quantum dot induced by the simultaneous oscillations of the impurity coordinate and spatial stretch of the impurity domain. We have considered repulsive Gaussian impurity centers. The ratio of two oscillations (η) has been exploited to understand the nature of the excitation rate. Indeed, it has been found that the said ratio could orchestrate the excitation in a most elegant way. In conjunction with the ratio, the dopant location also plays some important role towards modulating the excitation rate. The present study also indicates attainment of stabilization in the excitation rate as soon as η exceeds a threshold value irrespective of the dopant location. Moreover, prior to the onset of stabilization, we also envisage maximization/minimization in the excitation rate at some typical η values depending on the dopant location. The critical dissection of the characteristics of various impurity parameters provides important insight into the physics underlying the excitation process.

Keywords: Quantum dot, Impurity domain, Impurity coordinate, Impurity propagation, Excitation rate

Background

Nowadays, we envisage an upsurge in theoretical and experimental researches on impurity states of low-dimensional heterostructures [1]. The quantized properties of these doped systems have made them perfect objects for scientific study and technological applications. In view of this, researches on optoelectronic properties of a wide range of semiconductor devices containing impurity now turn out to be a highly pursued area [2-4].

Miniaturization of semiconductor devices reaches its limit with the advent of quantum dots (QDs). With QDs, the subtle interplay between new confinement sources and impurity-related potentials has opened up new windows of research in this field [5]. Such confinement, coupled with the dopant location, can dramatically alter the electronic and optical properties of the system [6]. For this reason, there are a seemingly large number of theoretical studies on impurity states [7-11]. Specifically, there are some important studies that emphasize the role of dopant location in influencing the dot properties [12,13]. Investigations on fabricating the impurity states have received further impetus with the development of sophisticated experimental techniques such as molecular beam epitaxy, liquid phase epitaxy, and chemical vapor deposition. Inspired by these, a series of elegant experiments on impurity-doped quantum dot systems resulted in some promising outcomes. These involve primarily the mechanism and control of dopant incorporation [14,15].

The application of new experimental and theoretical techniques together with the improvement of traditional ones has resulted in a great surge in the knowledge of carrier dynamics in nanodevices [16]. The time-dependent aspects in nanodevices naturally become a hot topic which largely comprises of researches on internal transitions between impurity-induced states in a QD. These transitions depend on the spatial restriction imposed by the impurity. As a natural consequence of the said research,

*Correspondence: pcmg77@rediffmail.com
[2]Physical Chemistry Section, Department of Chemistry, Visva Bharati University, Santiniketan, Birbhum, West Bengal, 731235, India
Full list of author information is available at the end of the article

the *excitation* of electrons strongly confined by QDs emanates as an interesting phenomenon that is intimately related to the above dynamical features. Detailed analysis on this aspect is undoubtedly of prime importance because such excitation provides us with ideal systems for use in optoelectronic devices and as lasers. Engineering applications of such excitations further involve optical encoding, multiplexing, photovoltaic, and light-emitting devices. Another aspect that makes excitation phenomenon so much important in QD is the eventual population transfer among the exciton states [17].

Studies on impurity propagation in doped quantum dots are going in full swing nowadays. The impurities can be incorporated by diffusion [18], and they experience some kind of force offered by the dot confinement potential [19]. Sundqvist et al., in their work [20], considered diffusion of ionized impurities interacting with electrons experimentally. In their work, the impurity profiles in low-dimensional structures were regulated by an external parabolic potential defined by a variety of gate arrangements, and they maintained impurity profiles of a typical Gaussian shape. The importance of studying such time-dependent propagation of dopant site lies in the fact that it could be correlated to the impurity drift in semiconductor nanodevices which has attracted a great deal of interest as most low-dimensional structures contain doped regions. The aspects discussed so far have motivated us to investigate thoroughly the excitation in doped quantum dots which is induced by a time-dependent propagation of the dopant coordinate. As a result, recently, we have made such an investigation where the propagation of the dopant has been considered to be linear as well as random [21,22]. In this paper, we have tried to extend our work a bit further by considering a periodic motion of the dopant. Such periodic motion could have its origin in the crystal lattice where the dopant is subject to some periodic force. To make the work more meaningful, we have also considered the periodic oscillation in the spatial stretch of the dopant (denoted by symbol γ in this paper) which is intimately related to the confinement strength. This deeper physical insight is a must as a periodically propagating dopant is obviously subject to a periodically strengthening and weakening confinement which forces the spatial spread of the dopant to respond accordingly and not to remain indifferent. Thus, notwithstanding the tedious hike in the mathematical rigor, consideration of a consequent periodic stretching and quenching of spatial spread of impurity appears highly logical. In view of this, the impurity coordinate (x_0, y_0) is allowed to oscillate with frequency (ν_1), enjoying the company of oscillatory γ with frequency $(\nu_2 = \frac{\nu_1}{\eta}, \eta =$ integers and fractions). To be precise, in this paper, we have monitored the ratio of the above two oscillation frequencies (termed as relative oscillation frequency, ROF) in connection with determining the time-average excitation rate for different dopant locations. Following earlier works on the effects of a repulsive scatterer in multicarrier dots in the presence of a magnetic field [23,24], here, we have considered that the QD is doped with a repulsive Gaussian impurity. The present formalism tackles the time dependencies by introducing a potential $V(t)$ to the dot Hamiltonian. The problem therefore rides on following the dynamics of the doped dot in the time-dependent potential.

Method

We consider the energy eigenstates of an electron subject to a harmonic confinement potential $V(x, y)$ and a perpendicular magnetic field B where $V(x, y) = \frac{1}{2}m^*\omega_0^2(x^2 + y^2)$, $\omega_c = \frac{eB}{m^*c}$, and Landau gauge $[A = (By, 0, 0)]$ has been used. ω_0, ω_c, and A stand for harmonic confinement potential, cyclotron frequency (a measure of magnetic confinement offered by B), and vector potential, respectively. The Hamiltonian in our problem reads

$$H_0' = -\frac{\hbar^2}{2m^*}\left(\frac{\partial^2}{\partial x^2}+\frac{\partial^2}{\partial y^2}\right)+\frac{1}{2}m^*\omega_0^2x^2+\frac{1}{2}m^*(\omega_0^2+\omega_c^2)y^2 - i\hbar\omega_c y\frac{\partial}{\partial x}. \tag{1}$$

Define $\Omega^2 = \omega_0^2 + \omega_c^2$ as the effective frequency in the y-direction. In real QDs, the electrons are confined in three dimensions, i.e., the carriers are dynamically confined to zero dimensions. The confinement length scales R^1, R^2, and R^3 can be different in three spatial directions, but typically $R^3 \ll R^1 \simeq R^2$. In models of such dots, R^3 is often taken to be strictly zero, and the confinement in the other two directions is described by a potential V with $V(x) \to \infty$ for $|x| \to \infty$, $x = (x^1, x^2) \in R^2$. A parabolic potential, $V = \frac{1}{2}\omega|x|^2$ is often used as a realistic and, at the same time, computationally convenient approximation. Assuming that the z-extension could be effectively considered zero, the electronic properties in these nanostructures have been successfully described within the model of the single-electron motion in the two-dimensional (2-d) harmonic oscillator potential in the presence of a magnetic field [25,26]. Now, intrusion of impurity perturbation transforms the Hamiltonian to

$$H_0(x, y, \omega_c, \omega_0) = H_0'(x, y, \omega_c, \omega_0) + V_{\text{imp}}(x_0, y_0), \tag{2}$$

where $V_{\text{imp}}(x_0, y_0) = V_{\text{imp}}(0) = V_0\ e^{-\gamma[(x-x_0)^2+(y-y_0)^2]}$ with $\gamma > 0$ and $V_0 > 0$ for repulsive impurity, and (x_0, y_0) denotes the position of the impurity center. V_0 is a measure of the strength of the impurity potential, whereas γ determines the extent of influence of the impurity potential. A large value of γ indicates that the spatial extension of the impurity potential is highly restricted, whereas a small γ accounts for a spatially diffused one.

Thus, a change in γ in turn causes a change in the extent of the dot-impurity overlap that affects the excitation pattern noticeably [21]. The presence of repulsive scatterer simulates the dopant with excess electrons. The choice of a Gaussian impurity potential is not arbitrary as it has been exploited by several investigators [27-29]. In this context, the work of Gharaati et al. [30] merits mention. They proposed a new confinement potential for the spherical QDs called *modified Gaussian potential, MGP,* and showed that the new potential is suitable for predicting the spectral energy and wave functions of a spherical quantum dot.

We write the trial wave function $\psi(x,y)$ as a superposition of the product of harmonic oscillator eigenfunctions $\phi_n(\alpha x)$ and $\phi_m(\beta y)$, respectively, as follows:

$$\psi(x,y) = \sum_{n,m} C_{n,m}\phi_n(\alpha x)\phi_m(\beta y), \tag{3}$$

where $C_{n,m}$ are the variational parameters, and $\alpha = \sqrt{\frac{m^*\omega_0}{\hbar}}$ and $\beta = \sqrt{\frac{m^*\Omega}{\hbar}}$. The general expression for the matrix elements of H_0' in the chosen basis is as follows:

$$\begin{aligned}(H_0')_{n,m;n',m'} = \hbar\left\{\left(n'+\frac{1}{2}\right)\omega_0+\left(m'+\frac{1}{2}\right)\sqrt{\omega_0^2+\omega_c^2}\right\}\delta_{n,n'}\delta_{m,m'} \\ - i\hbar\omega_c\frac{\alpha}{\beta}\left[\left\{\sqrt{\frac{n'}{2}}\delta_{n'-1,n}-\sqrt{\frac{n'+1}{2}}\delta_{n'+1,n}\right\}\cdot\right. \\ \left.\left\{\sqrt{\frac{m'+1}{2}}\delta_{m'+1,m}+\sqrt{\frac{m'}{2}}\delta_{m'-1,m}\right\}\right].\end{aligned} \tag{4}$$

The matrix elements of V_{imp} are given by

$$\begin{aligned}(V_{\text{imp}})_{n,m;n',m'} &= V_0\langle\phi_n(\alpha x)\phi_m(\beta y)|e^{-\gamma[(x-x_0)^2+(y-y_0)^2]} \\ &\quad\times|\phi_{n'}(\alpha x)\phi_{m'}(\beta y)\rangle \\ &= V_0 I_1 I_2,\end{aligned} \tag{5}$$

where

$$\begin{aligned}I_1 &= \langle\phi_n(\alpha x)|e^{-\gamma(x-x_0)^2}|\phi_n'(\alpha x)\rangle \\ &= A\int_{-\infty}^{+\infty} H_n(\alpha x)H_{n'}(\alpha x)e^{-\alpha^2x^2}e^{-\gamma(x-x_0)^2}dx,\end{aligned} \tag{6}$$

and

$$\begin{aligned}I_2 &= \langle\phi_m(\beta y)|e^{-\gamma(y-y_0)^2}|\phi_m'(\beta y)\rangle \\ &= B\int_{-\infty}^{+\infty} H_m(\beta y)H_{m'}(\beta y)e^{-\beta^2y^2}e^{-\gamma(y-y_0)^2}dy,\end{aligned} \tag{7}$$

with $A = \frac{\alpha}{(2^{n+n'}n!n'!\pi)^{1/2}}$ and $B = \frac{\beta}{(2^{m+m'}m!m'!\pi)^{1/2}}$. With the transformations $\delta_1^2 = \alpha^2+\gamma$, $\delta_2^2 = \beta^2+\gamma$, $\lambda_1 = \exp[-\frac{\gamma x_0^2(\delta_1^2-\gamma)}{\delta_1^2}]$, and $\lambda_2 = \exp[-\frac{\gamma y_0^2(\delta_2^2-\gamma)}{\delta_2^2}]$, one can write

$$I_1 = A\lambda_1\int_{-\infty}^{+\infty} H_n(\alpha^*u)H_{n'}(\alpha^*u)e^{-(u-\rho_1)^2}du, \tag{8}$$

and

$$I_2 = B\lambda_2\int_{-\infty}^{+\infty} H_m(\beta^*v)H_{m'}(\beta^*v)e^{-(v-\rho_2)^2}dv, \tag{9}$$

where, $\rho_1 = \frac{\gamma x_0}{\delta_1}$, $\rho_2 = \frac{\gamma y_0}{\delta_2}$, $\alpha^* = \frac{\alpha}{\delta_1}$, $\beta^* = \frac{\beta}{\delta_2}$, $u = \delta_1 x$, and $v = \delta_2 y$. With the help of the standard integral [31], it is now easy to write

$$I_1 = D_1\sum_{k=0}^{\min(n,n')} f(k,n,n'), \tag{10}$$

and

$$I_2 = D_2\sum_{l=0}^{\min(m,m')} g(l,m,m'), \tag{11}$$

where

$$f(k,n,n') = 2^k.k!.{}^nC_k.{}^{n'}C_k.(1-\alpha^{*2})^{\frac{n+n'}{2}-k}.H_{n+n'-2k}(\alpha_1\rho_1), \tag{12}$$

and

$$g(l,m,m') = 2^l.l!.{}^mC_l.{}^{m'}C_l.(1-\beta^{*2})^{\frac{m+m'}{2}-l}.H_{m+m'-2l}(\beta_1\rho_2), \tag{13}$$

with $D_1 = \frac{A\lambda_1\pi^{1/2}}{\delta_1}$ and $D_2 = \frac{B\lambda_2\pi^{1/2}}{\delta_2}$. Thus, finally we obtain

$$\begin{aligned}(V_{\text{imp}})_{n,m;n',m'} = V_0.D_1.D_2.\sum_{k=0}^{\min(n,n')}\sum_{l=0}^{\min(m,m')} f(k,n,n').\\ \times g(l,m,m').\end{aligned} \tag{14}$$

$H_n(x)$ stands for the Hermite polynomials of the nth order. The pth eigenstate of the system in this representation can be written as

$$\psi_p(x,y) = \sum_{ij} C_{ij,p}\{\phi_i(\alpha x)\phi_j(\beta y)\}, \tag{15}$$

where i, j are the appropriate quantum numbers, respectively, and (ij) are composite indices specifying the direct product basis.

We can now introduce the time dependence into the dopant coordinate so that $x_0 \to x_0(t)$ and $y_0 \to y_0(t)$. Now, the time-dependent Hamiltonian reads

$$H(t) = [H_0 - V_{\text{imp}}(0)] + V_1(t), \tag{16}$$

where

$$V_1(t) = V_{\text{imp}}[x_0(t), y_0(t)] = V_0\, e^{-\gamma[\{x-x_0(t)\}^2+\{y-y_0(t)\}^2]}. \tag{17}$$

The matrix element involving any two arbitrary eigenstates p and q of H_0 due to $V_1(t)$ reads

$$V_{p,q}^{\text{imp}}(t) = \langle \psi_p(x,y)|V_1(t)|\psi_q(x,y)\rangle = \sum_{nm}\sum_{n'm'} C^*_{nm,p}C_{n'm',q}\langle \phi_n(\alpha x)\phi_m(\beta y)|V_1(t)|\phi_{n'} \times (\alpha x)\phi_{m'}(\beta y)\rangle. \quad (18)$$

Denoting $V_1^{n,m,n',m'}(t)$ to represent $\langle \phi_n(\alpha x)\phi_m(\beta y)|V_1(t)|\phi_{n'}(\alpha x)\phi_{m'}(\beta y)\rangle$, its explicit form could be written as (with the help of Equations 5 to 14)

$$V_1^{n,m,n',m'}(t) = V_0.\Delta_1.\Delta_2.\lambda_1(t).\lambda_2(t) \sum_{k=0}^{\min(n,n')}\sum_{l=0}^{\min(m,m')} \times f_{k,n,n'}(t).g_{l,m,m'}(t), \quad (19)$$

where

$$f_{k,n,n'}(t) = 2^k.k!.{}^nC_k.{}^{n'}C_k.(1-\alpha^{*2})^{\frac{n+n'}{2}-k}H_{n+n'-2k}[\alpha_1\rho_1(t)],$$

and

$$g_{l,m,m'}(t) = 2^l.l!.{}^mC_l.{}^{m'}C_l.(1-\beta^{*2})^{\frac{m+m'}{2}-l}H_{m+m'-2l} \times[\beta_1\rho_2(t)].$$

The terms that are not defined previously read as follows: $\Delta_1 = A\pi^{1/2}$, $\Delta_2 = B\pi^{1/2}$, $\lambda_1(t) = \exp[-\frac{\gamma x_0^2(t)\alpha^2}{\delta_1^2}]$, $\lambda_2(t) = \exp[-\frac{\gamma y_0^2(t)\beta^2}{\delta_2^2}]$, $\rho_1(t) = \frac{\gamma x_0(t)}{\delta_1}$, and $\rho_2(t) = \frac{\gamma y_0(t)}{\delta_2}$. Thus, Equation 18 becomes

$$V_{p,q}^{\text{imp}}(t) = V_0\lambda_1(t)\lambda_2(t)\sum_{nm}\sum_{n'm'}C^*_{nm,p}C_{n'm',q}\Delta_1\Delta_2 \times \sum_{k=0}^{\min(n,n')}\sum_{l=0}^{\min(m,m')} f_{k,n,n'}(t).g_{l,m,m'}(t). \quad (20)$$

Considering $\rho_1(t)$ and $\rho_2(t)$ to be extremely slowly varying functions of time, we could expand them in Taylor series around $t = 0$ and neglect the nonlinear terms to obtain

$$\begin{aligned} &H_{n+n'-2k}[\alpha_1\rho_1(t)]\ H_{m+m'-2l}[\beta_1\rho_2(t)] \\ &= H_{n+n'-2k}[\alpha_1\rho_1(0)]H_{m+m'-2l}[\beta_1\rho_2(0)] \\ &\quad + 2t\alpha_1\rho_1'(0)(n+n'-2k)H_{n+n'-2k-1}[\alpha_1\rho_1(0)] \\ &\quad \times H_{m+m'-2l}[\beta_1\rho_2(0)] \\ &\quad + 2t\beta_1\rho_2'(0)(m+m'-2l)H_{m+m'-2l-1}[\beta_1\rho_2(0)] \\ &\quad \times H_{n+n'-2k}[\alpha_1\rho_1(0)] \\ &\quad + 4t^2\alpha_1\beta_1\rho_1'(0)\rho_2'(0)(n+n'-2k)(m+m'-2l) \\ &\quad \times H_{n+n'-2k-1}[\alpha_1\rho_1(0)]H_{m+m'-2l-1}[\beta_1\rho_2(0)], \end{aligned} \quad (21)$$

where we have utilized the well-known property of the derivatives of the Hermite polynomial *viz.* $H_n'(x) = 2nH_{n-1}(x)$. Using Equation 21 in Equation 20, we get Equation 22 *viz.*

$$V_{p,q}^{\text{imp}}(t) = V_0\left[V_{p,q}^1(t) + V_{p,q}^2(t) + V_{p,q}^3(t) + V_{p,q}^4(t)\right], \quad (22)$$

where the various terms are as follows:

$$V_{p,q}^1(t) = \lambda_1(t)\lambda_2(t)\sum_{nm}\sum_{n'm'}C^*_{nm,p}C_{n'm',q}\Delta_1\Delta_2 \cdot \sum_{k=0}^{\min(n,n')}\sum_{l=0}^{\min(m,m')} f_{k,n,n'}(0).g_{l,m,m'}(0), \quad (23)$$

$$V_{p,q}^2(t) = 2t\alpha_1\rho_1'(0)\lambda_1(t)\lambda_2(t)\sum_{nm}\sum_{n'm'}C^*_{nm,p}C_{n'm',q}\Delta_1\Delta_2 \cdot \sum_{k=0}^{\min(n,n')}\sum_{l=0}^{\min(m,m')} u_{k,n,n'}(0).g_{l,m,m'}(0), \quad (24)$$

with $u_{k,n,n'}(0) = 2^k.k!.{}^nC_k.{}^{n'}C_k.(n+n'-2k)(1-\alpha^{*2})^{\frac{n+n'}{2}-k}H_{n+n'-2k-1}[\alpha_1\rho_1(0)]$.

$$V_{p,q}^3(t) = 2t\beta_1\rho_2'(0)\lambda_1(t)\lambda_2(t)\sum_{nm}\sum_{n'm'}C^*_{nm,p}C_{n'm',q}\Delta_1\Delta_2 \cdot \sum_{k=0}^{\min(n,n')}\sum_{l=0}^{\min(m,m')} f_{k,n,n'}(0).\nu_{l,m,m'}(0), \quad (25)$$

with $\nu_{l,m,m'}(0) = 2^l.l!.{}^mC_l.{}^{m'}C_l.(m+m'-2l)(1-\beta^{*2})^{\frac{m+m'}{2}-l}H_{m+m'-2l-1}[\beta_1\rho_2(0)]$.

$$V_{p,q}^4(t) = 4t^2\alpha_1\beta_1\rho_1'(0)\rho_2'(0)\lambda_1(t)\lambda_2(t)\sum_{nm}\sum_{n'm'}C^*_{nm,p} \times C_{n'm',q}\Delta_1\Delta_2.\sum_{k=0}^{\min(n,n')}\sum_{l=0}^{\min(m,m')} \times u_{k,n,n'}(0).\nu_{l,m,m'}(0). \quad (26)$$

The time-dependent periodic propagation of the dopant is represented as $x_0(t) = x_0\cos(\nu_1 t)$, and $y_0(t) = y_0\cos(\nu_1 t)$. Now, we introduce the accompanying periodic time dependence in γ as a result of oscillatory dopant propagation given by $\gamma(t) = \gamma_0\cos(\nu_2 t)$, γ_0 is the initial value of γ. Thus, it is nothing but a sluggish alternating enhancement and suppression of the region over which the influence of the dopant is disseminated owing to its drift. The introduction of the time dependence into the impurity domain ($\gamma_0 \rightarrow \gamma(t)$) modifies $V_1(t)$ of Equation 16 so that it becomes

$$V_1(t) = V_0\, e^{-\gamma(t)\left[\{x-x_0(t)\}^2+\{y-y_0(t)\}^2\right]}. \quad (27)$$

$V_1^{n,m,n',m'}(t)$ of Equation 19 now reads

$$V_1^{n,m,n',m'}(t) = V_0.\Delta_1.\Delta_2.U_1(t).U_2(t) \sum_{k=0}^{\min(n,n')} \sum_{l=0}^{\min(m,m')} \times \zeta_{k,n,n'}(t).\chi_{l,m,m'}(t), \tag{28}$$

where

$$\zeta_{k,n,n'}(t) = 2^k.k!.{}^nC_k.{}^{n'}C_k.\{w_1(t)\}^{g_1}\ H_{g_3}[\nu_1(t)],$$

and

$$\chi_{l,m,m'}(t) = 2^l.l!.{}^mC_l.{}^{m'}C_l.\{w_2(t)\}^{g_2}\ H_{g_4}[\nu_2(t)].$$

The relevant quantities now assume some modified expressions and read as follows: $\delta_1^2(t) = \alpha^2 + \gamma(t)$, $\delta_2^2(t) = \beta^2 + \gamma(t)$, with $\lambda_1(t) = \exp[-\frac{\gamma(t)x_0^2(t)\alpha^2}{\delta_1^2(t)}]$, $\lambda_2(t) = \exp[-\frac{\gamma(t)y_0^2(t)\beta^2}{\delta_2^2(t)}]$, $w_1(t) = \frac{\gamma(t)}{\delta_1^2(t)}$, $w_2(t) = \frac{\gamma(t)}{\delta_2^2(t)}$, $U_1(t) = \frac{\lambda_1(t)}{\delta_1(t)}$, $U_2(t) = \frac{\lambda_2(t)}{\delta_2(t)}$, $\nu_1(t) = \frac{\alpha x_0(t)\sqrt{\gamma(t)}}{\delta_1(t)}$, $\nu_2(t) = \frac{\beta y_0(t)\sqrt{\gamma(t)}}{\delta_2(t)}$, $g_1 = \frac{n+n'}{2} - k$, $g_2 = \frac{m+m'}{2} - l$, $g_3 = n + n' - 2k$, and $g_4 = m + m' - 2l$. Thus, Equation 20 now becomes

$$V_{p,q}^{\text{imp}}(t) = V_0 U_1(t)U_2(t) \sum_{nm}\sum_{n'm'} C^*_{nm,p}C_{n'm',q}\Delta_1\Delta_2 \times \sum_{k=0}^{\min(n,n')} \sum_{l=0}^{\min(m,m')} \zeta_{k,n,n'}(t).\chi_{l,m,m'}(t). \tag{29}$$

As before, we allow the time-dependent functions *viz.* $w_1(t)$, $w_2(t)$, $\nu_1(t)$, and $\nu_2(t)$ to vary extremely slowly with time so that we can expand them in Taylor series around $t = 0$ and neglect the nonlinear terms to obtain

$$\begin{aligned}
&[w_1(t)]^{g_1}\,[w_2(t)]^{g_2}\,H_{g_3}[\nu_1(t)]\,H_{g_4}[\nu_2(t)]\\
&=[w_1(0)]^{g_1}\,[w_2(0)]^{g_2}\,\big[\{\varphi_1(0) + 2tg_3\varphi_2(0)\\
&\quad + 2tg_4\varphi_3(0) + 4t^2g_3g_4\varphi_4(0)\} + \{tg_1\theta_1(0)\varphi_1(0)\\
&\quad +2t^2g_1g_3\theta_1(0)\varphi_2(0) + 2t^2g_1g_4\theta_1(0)\varphi_3(0)\\
&\quad + 4t^3g_1g_3g_4\theta_1(0)\varphi_4(0)\} + \{tg_2\theta_2(0)\varphi_1(0)\\
&\quad + 2t^2g_2g_3\theta_2(0)\varphi_2(0) + 2t^2g_2g_4\theta_2(0)\varphi_3(0)\\
&\quad + 4t^3g_2g_3g_4\theta_2(0)\varphi_4(0)\} + \{t^2g_1g_2\theta_3(0)\varphi_1(0)\\
&\quad + 2t^3g_1g_2g_3\theta_3(0)\varphi_2(0) + 2t^3g_1g_2g_4\theta_3(0)\varphi_3(0)\\
&\quad + 4t^4g_1g_2g_3g_4\theta_3(0)\varphi_4(0)\}\big],
\end{aligned} \tag{30}$$

where $\theta_1(0) = \frac{w_1'(0)}{w_1(0)}$, $\theta_2(0) = \frac{w_2'(0)}{w_2(0)}$, $\theta_3(0) = \theta_1(0)\theta_2(0)$, $\varphi_1(0) = H_{g_3}[\nu_1(0)].H_{g_4}[\nu_2(0)]$, $\varphi_2(0) = \nu_1'(0)H_{g_3-1}[\nu_1(0)].H_{g_4}[\nu_2(0)]$, $\varphi_3(0) = \nu_2'(0)H_{g_3}[\nu_1(0)].H_{g_4-1}[\nu_2(0)]$, and $\varphi_4(0) = \nu_1'(0)\nu_2'(0)H_{g_3-1}[\nu_1(0)].H_{g_4-1}[\nu_2(0)]$ (using the property $H_n'(x) = 2nH_{n-1}(x)$). Using Equation 30 in Equation 29, we get

$$V_{p,q}^{\text{imp}}(t) = V_0\sum_{j=1}^{16} V_{p,q}^j(t), \tag{31}$$

where the various $V_{p,q}^j(t)$ terms are as follows:

$$V_{p,q}^1(t) = U_1(t)U_2(t)\sum_{nm}\sum_{n'm'} C^*_{nm,p}C_{n'm',q}\Delta_1\Delta_2 \times \sum_{k=0}^{\min(n,n')} \sum_{l=0}^{\min(m,m')} \xi_1(0), \tag{32}$$

$$V_{p,q}^2(t) = 2tU_1(t)U_2(t)\sum_{nm}\sum_{n'm'} C^*_{nm,p}C_{n'm',q}\Delta_1\Delta_2 \times \sum_{k=0}^{\min(n,n')} \sum_{l=0}^{\min(m,m')} \xi_2(0), \tag{33}$$

$$V_{p,q}^3(t) = 2tU_1(t)U_2(t)\sum_{nm}\sum_{n'm'} C^*_{nm,p}C_{n'm',q}\Delta_1\Delta_2 \times \sum_{k=0}^{\min(n,n')} \sum_{l=0}^{\min(m,m')} \xi_3(0), \tag{34}$$

$$V_{p,q}^4(t) = 4t^2U_1(t)U_2(t)\sum_{nm}\sum_{n'm'} C^*_{nm,p}C_{n'm',q}\Delta_1\Delta_2 \times \sum_{k=0}^{\min(n,n')} \sum_{l=0}^{\min(m,m')} \xi_4(0), \tag{35}$$

$$V_{p,q}^5(t) = tU_1(t)U_2(t)\theta_1(0)\sum_{nm}\sum_{n'm'} C^*_{nm,p}C_{n'm',q}\Delta_1\Delta_2 \times \sum_{k=0}^{\min(n,n')} \sum_{l=0}^{\min(m,m')} \xi_5(0), \tag{36}$$

$$V_{p,q}^6(t) = 2t^2U_1(t)U_2(t)\theta_1(0)\sum_{nm}\sum_{n'm'} C^*_{nm,p}C_{n'm',q}\Delta_1\Delta_2 \times \sum_{k=0}^{\min(n,n')} \sum_{l=0}^{\min(m,m')} \xi_6(0), \tag{37}$$

$$V_{p,q}^7(t) = 2t^2U_1(t)U_2(t)\theta_1(0)\sum_{nm}\sum_{n'm'} C^*_{nm,p}C_{n'm',q}\Delta_1\Delta_2 \times \sum_{k=0}^{\min(n,n')} \sum_{l=0}^{\min(m,m')} \xi_7(0), \tag{38}$$

$$V_{p,q}^{8}(t) = 4t^3 U_1(t)U_2(t)\theta_1(0)\sum_{nm}\sum_{n'm'} C_{nm,p}^{*} C_{n'm',q}\Delta_1\Delta_2 \times \sum_{k=0}^{\min(n,n')}\sum_{l=0}^{\min(m,m')} \xi_8(0), \tag{39}$$

$$V_{p,q}^{9}(t) = tU_1(t)U_2(t)\theta_2(0)\sum_{nm}\sum_{n'm'} C_{nm,p}^{*} C_{n'm',q}\Delta_1\Delta_2 \times \sum_{k=0}^{\min(n,n')}\sum_{l=0}^{\min(m,m')} \xi_9(0), \tag{40}$$

$$V_{p,q}^{10}(t) = 2t^2 U_1(t)U_2(t)\theta_2(0)\sum_{nm}\sum_{n'm'} C_{nm,p}^{*} C_{n'm',q}\Delta_1\Delta_2 \times \sum_{k=0}^{\min(n,n')}\sum_{l=0}^{\min(m,m')} \xi_{10}(0), \tag{41}$$

$$V_{p,q}^{11}(t) = 2t^2 U_1(t)U_2(t)\theta_2(0)\sum_{nm}\sum_{n'm'} C_{nm,p}^{*} C_{n'm',q}\Delta_1\Delta_2 \times \sum_{k=0}^{\min(n,n')}\sum_{l=0}^{\min(m,m')} \xi_{11}(0), \tag{42}$$

$$V_{p,q}^{12}(t) = 4t^3 U_1(t)U_2(t)\theta_2(0)\sum_{nm}\sum_{n'm'} C_{nm,p}^{*} C_{n'm',q}\Delta_1\Delta_2 \times \sum_{k=0}^{\min(n,n')}\sum_{l=0}^{\min(m,m')} \xi_{12}(0), \tag{43}$$

$$V_{p,q}^{13}(t) = t^2 U_1(t)U_2(t)\theta_3(0)\sum_{nm}\sum_{n'm'} C_{nm,p}^{*} C_{n'm',q}\Delta_1\Delta_2 \times \sum_{k=0}^{\min(n,n')}\sum_{l=0}^{\min(m,m')} \xi_{13}(0), \tag{44}$$

$$V_{p,q}^{14}(t) = 2t^3 U_1(t)U_2(t)\theta_3(0)\sum_{nm}\sum_{n'm'} C_{nm,p}^{*} C_{n'm',q}\Delta_1\Delta_2 \times \sum_{k=0}^{\min(n,n')}\sum_{l=0}^{\min(m,m')} \xi_{14}(0), \tag{45}$$

$$V_{p,q}^{15}(t) = 2t^3 U_1(t)U_2(t)\theta_3(0)\sum_{nm}\sum_{n'm'} C_{nm,p}^{*} C_{n'm',q}\Delta_1\Delta_2 \times \sum_{k=0}^{\min(n,n')}\sum_{l=0}^{\min(m,m')} \xi_{15}(0), \tag{46}$$

and

$$V_{p,q}^{16}(t) = 4t^4 U_1(t)U_2(t)\theta_3(0)\sum_{nm}\sum_{n'm'} C_{nm,p}^{*} C_{n'm',q}\Delta_1\Delta_2 \times \sum_{k=0}^{\min(n,n')}\sum_{l=0}^{\min(m,m')} \xi_{16}(0). \tag{47}$$

The various ξ functions are as follows: $\xi_1(0) = [w_1(0)]^{g_1}[w_2(0)]^{g_2}\varphi_1(0)$, $\xi_2(0) = [w_1(0)]^{g_1}[w_2(0)]^{g_2} g_3\varphi_2(0)$, $\xi_3(0) = [w_1(0)]^{g_1}[w_2(0)]^{g_2} g_4\varphi_3(0)$, $\xi_4(0) = [w_1(0)]^{g_1}[w_2(0)]^{g_2} g_3g_4\varphi_4(0)$, $\xi_5(0) = [w_1(0)]^{g_1}[w_2(0)]^{g_2} g_1\varphi_1(0)$, $\xi_6(0) = [w_1(0)]^{g_1}[w_2(0)]^{g_2} g_1g_3\varphi_2(0)$, $\xi_7(0) = [w_1(0)]^{g_1}[w_2(0)]^{g_2} g_1g_4\varphi_3(0)$, $\xi_8(0) = [w_1(0)]^{g_1}[w_2(0)]^{g_2} g_1g_3g_4\varphi_4(0)$, $\xi_9(0) = [w_1(0)]^{g_1}[w_2(0)]^{g_2} g_2\varphi_1(0)$, $\xi_{10}(0) = [w_1(0)]^{g_1}[w_2(0)]^{g_2} g_2g_3\varphi_2(0)$, $\xi_{11}(0) = [w_1(0)]^{g_1}[w_2(0)]^{g_2} g_2g_4\varphi_3(0)$, $\xi_{12}(0) = [w_1(0)]^{g_1}[w_2(0)]^{g_2} g_2g_3g_4\varphi_4(0)$, $\xi_{13}(0) = [w_1(0)]^{g_1}[w_2(0)]^{g_2} g_1g_2\varphi_1(0)$, $\xi_{14}(0) = [w_1(0)]^{g_1}[w_2(0)]^{g_2} g_1g_2g_3\varphi_2(0)$, $\xi_{15}(0) = [w_1(0)]^{g_1}[w_2(0)]^{g_2} g_1g_2g_4\varphi_3(0)$, and $\xi_{16}(0) = [w_1(0)]^{g_1}[w_2(0)]^{g_2} g_1g_2g_3g_4\varphi_4(0)$. The $w(t)$ and $\nu(t)$ functions grossly look like $w_1(t) = \frac{\gamma(t)}{\alpha^2+\gamma(t)}$, $w_2(t) = \frac{\gamma(t)}{\beta^2+\gamma(t)}$, $\nu_1(t) = \alpha x_0(t)\sqrt{\frac{\gamma(t)}{\alpha^2+\gamma(t)}}$, and $\nu_2(t) = \beta y_0(t)\sqrt{\frac{\gamma(t)}{\beta^2+\gamma(t)}}$. The pertinent derivative functions read $w_1'(t) = -\frac{\alpha^2\nu_2\gamma_0\sin(\nu_2 t)}{[\alpha^2+\gamma(t)]^2}$, $w_2'(t) = -\frac{\beta^2\nu_2\gamma_0\sin(\nu_2 t)}{[\beta^2+\gamma(t)]^2}$, $\nu_1'(t) = \frac{\frac{1}{2}\alpha x_0(t)\nu_2\gamma_0\sin(\nu_2 t)\left[\sqrt{\frac{\gamma(t)}{\alpha^2+\gamma(t)}} - \sqrt{\frac{\alpha^2+\gamma(t)}{\gamma(t)}}\right] - \alpha x_0\nu_1\sin(\nu_1 t)\sqrt{\gamma(t)\{\alpha^2+\gamma(t)\}}}{\alpha^2+\gamma(t)}$, and $\nu_2'(t) = \frac{\frac{1}{2}\beta y_0(t)\nu_2\gamma_0\sin(\nu_2 t)\left[\sqrt{\frac{\gamma(t)}{\beta^2+\gamma(t)}} - \sqrt{\frac{\beta^2+\gamma(t)}{\gamma(t)}}\right] - \beta x_0\nu_1\sin(\nu_1 t)\sqrt{\gamma(t)\{\beta^2+\gamma(t)\}}}{\beta^2+\gamma(t)}$.

From these relations, explicit expressions of various θ and φ functions can be easily found out, thereby giving concrete expressions of $V_{p,q}^{\mathrm{imp}}(t)$ in Equation 31.

Since H_0 is diagonal in the $\{\psi\}$ basis, the evolving wave function can now be described by a superposition of the eigenstates of H_0.

$$\psi(x,y,t) = \sum_q a_q(t)\psi_q, \tag{48}$$

and we have to solve the TDSE.

$$i\hbar\frac{\partial\psi}{\partial t} = H\psi \quad \text{or} \quad \text{equivalently}$$

$$i\hbar\dot{a}_q(t) = Ha_q(t), \tag{49}$$

for the time-dependent superposition coefficients with the initial conditions that $a_p(0) = 1$, $a_q(0) = 0$, for all

$q \neq p$, where p may be the ground or any other excited states of H_0. The quantity $P_k(t) = |a_k(t)|^2$ could act as a measure of the population of the kth state of H_0 at time t. During the time evolution, the ground state population $[P_0(t)]$ fluctuates. We could define the quantity $Q(t) = 1 - P_0(t)$ as a measure of excitation. The quantity $R_{ex}(t) = \frac{dQ}{dt}$ serves as the rate of excitation as a function of time. We have calculated the average rate of excitation $[\langle R_{ex}\rangle = \frac{1}{T}\int_0^T R_{ex}(t)dt]$ over the total time of dynamic evolution (T) as a function of ROF (η) for different values of dopant locations (r_0).

Results and discussion

System parameters

The model Hamiltonian (*cf.* Equation 1) can be made to represent a 2-d quantum dot with a single carrier electron [32]. The form of the confinement potential indicates lateral electrostatic confinement of the electrons in the x-y plane. m^* is the effective electronic mass appropriate for describing the motion of the electrons within the lattice of the material to be used. We have used $m^* = 0.5m_0$ and set $\hbar = e = m_0 = a_0 = 1$. In the linear variational calculation, we have used basis functions (*cf.* Equation 3) with $n, m = 0 - 20$ for each of the directions (x, y). The direct product basis spans a space of (21×21) dimension. We have checked that the basis functions span the 2-d space effectively completely, at least with respect to representing the observables under investigation. We have made the convergence test with a still greater number of basis functions. The time-dependent Schrödinger equation in the direct product basis (*cf.* Equation 49) has been integrated by the sixth-order Runge-Kutta-Fehlberg method with a time step size $\Delta t = 0.01$ a.u., and the numerical stability of the integrator has been checked.

We have made some attempt to reasonably connect our theoretical parameters to the real-life doped QD. The dynamic evolution has been monitored through a time of the order of 100 ps. The parameter γ in the impurity potential can be correlated to $\frac{1}{d^2}$, where d is proportional to the width of the impurity potential [23,24] to have feelings of the actual extension of the impurity domain. The m^* value that we have used ($m^* = 0.5$ a.u.) closely resembles Ge quantum dots ($m^* = 0.55$ a.u.). The maximum value of the dopant strength (V_0) was limited to approximately 10^{-4} a.u. or 2.72 meV, and the applied magnetic field is of the order of miliTesla (mT). We believe that these values might give some realization of real systems containing actual impurity.

The dynamical aspects

At the very outset of the discussion, it needs to be realized that the excitation rate is modulated by the interplay between several factors of different characteristics. As the dopant is introduced at a greater distance from the dot confinement center $(0, 0)$, the confines of electric (ω_0) and magnetic (ω_c) origins naturally become weak and favor excitation. On the other hand, the said shift decreases the extent of repulsive interaction between the dot and the impurity, and excitation is unfavored. For a better visualization, we have plotted the matrix elements $\langle\psi_0|\hat{V}_{imp}|\psi_0\rangle$ as a function of the radial position of impurity (r_0) (Figure 1) to characterize the overlap of the impurity potential with the ground state wave function $|\psi_0\rangle$. The plot reveals that as the dopant is introduced away from the dot, their overlap decreases. However, at a large r_0, the overlap settles to a somewhat steady value. The spatial stretch of impurity (γ) has also a role to play in this context. An increase in γ reduces the spatial stretch of the impurity potential which in turn reduces the extent of overlap between the dot and the impurity. Such a decrease in the said overlap has a two-pronged role; primarily, it reduces the dot-impurity interaction and consequently the strength of dot confinement, thereby hindering and promoting the excitation at the same time [33]. Thus, the excitation process is often found to be guided by factors of opposite natures arising out of the variation of several impurity parameters.

Let us now have a close look at the plot that delineates the time-average excitation rate ($\langle R_{ex}\rangle$) as a function of ROF (η) for three different dopant locations, namely, on-center ($r_0 = 0.0$ a.u.), near off-center ($r_0 = 28.28$ a.u.), and far off-center ($r_0 = 70.71$ a.u.) (Figure 2). It is evident from the figure that at all dopant locations, the excitation rate culminates in a saturation at high η values, indicating a compromise between several factors that modulate the excitation. The diversities in the nature of

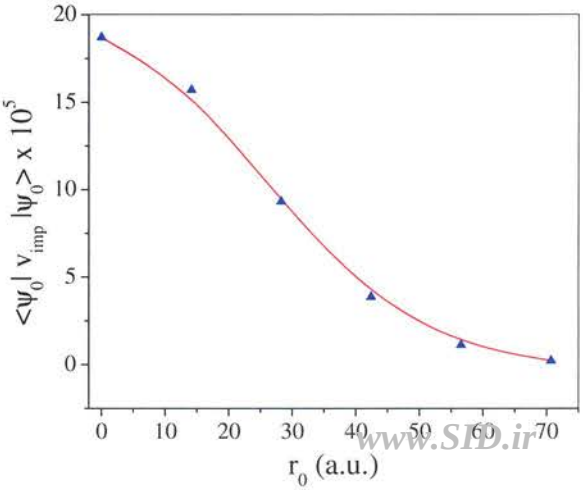

Figure 1 Plot of $\langle\psi_0|\hat{V}_{imp}|\psi_0\rangle$ against r_0.

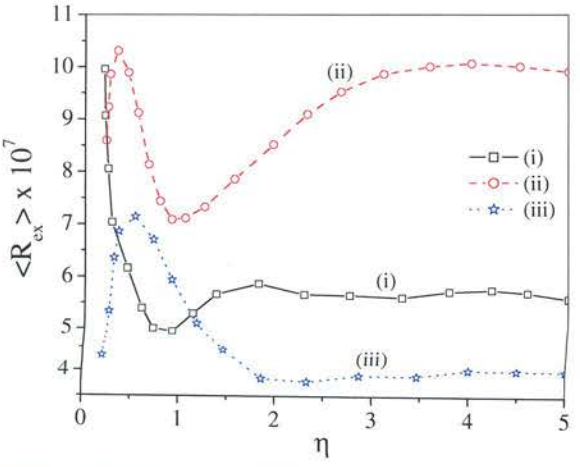

Figure 2 Plot of $\langle R_{ex} \rangle$ vs η for different dopant locations (r_0). With $\gamma_0 = 4.0 \times 10^{-6}$ a.u. and $V_0 = 1.0 \times 10^{-6}$ a.u. for (i) $r_0 = 0.0$ a.u., (ii) $r_0 = 28.28$ a.u., and (iii) $r_0 = 70.71$ a.u.

excitation profiles are most prominent in low and medium η values.

For an on-center dopant, it is evident that the excitation rate starts from a rather high value when η is extremely small. However, the rate falls noticeably to a minimum at around $\eta \sim 0.8$. With further increase in ROF, $\langle R_{ex} \rangle$ settles to a steady value. A low to low-medium η regime is endowed with a strong γ oscillation which, in the present case, seems to undergo a kind of skirmish with the oscillatory dopant coordinate. Thus, instead of promoting the excitation rate - which would have been possible if the two oscillations reinforce each other - we observe a depletion in the said quantity. Within the domain $0.91 \leq \eta \leq 1.78$, we observe a small rise in $\langle R_{ex} \rangle$, indicating a small reinforcement between the two oscillations. As η is gradually increased further (i.e., $\eta \geq 1.78$), the γ oscillation also becomes progressively less vocal (but yet it would be unwise to ignore it because of the on-center location of the dopant) and invites some semblance of balance between itself and the oscillation of r_0, leading to a saturation.

At a near off-center dopant location, the dot-impurity overlap gets somewhat reduced. Interestingly, at this dopant location, we envisage successive maximization (at $\eta \sim 0.34$) and minimization (at $\eta \sim 1.0$) of the excitation rate. Beyond $\eta \sim 0.5$, as usual, the excitation rate culminates in saturation. It appears that the two domains marked by maximization and minimization of the excitation rate are categorically distinguished from each other by simply a twist of relative behavior of r_0 and γ oscillations. However, looking at the placement of the dopant, one must acknowledge that, over the entire range of η, the influence of γ is not so much pronounced as it is in case of an on-center dopant. In the small η regime, the steep rise in $\langle R_{ex} \rangle$ indicates that the two oscillations reinforce each other. Beyond $\eta \sim 0.34$, there occurs a change in their relative attitude; they now begin to oppose each other and the rate decreases. Interestingly, the γ oscillation being not as strong as before (i.e., for on-center location), the fall in $\langle R_{ex} \rangle$ is not so severe as it is in the previous case. After minimization of the excitation rate, we again observe an increase in $\langle R_{ex} \rangle$ which is quite sluggish. This again indicates a kind of reinforcement among the two oscillations albeit not so strong as in the low η domain. The reduction in the extent of reinforcement can be explained by considering that in this domain ($1.05 \leq \eta \leq 3.10$), the γ oscillation becomes less vigorous in comparison with the low η domain so that it makes a weak combination with the r_0 oscillation.

For a far off-center dopant, we again find a maximization (at about $\eta \approx 0.51$) in the excitation rate just like the near off-center location. However, the extent of excitation is much less than before. At a far off-center dopant location, the dot-impurity overlap gets highly quenched so that the γ oscillation has little impact in comparison to the near off-center location. Even in the low η regime, where one usually expects the γ oscillation to be significant, we confront a nominal influence of the same, owing to such a depleted dot-impurity overlap. Thus, although we envisage the maximization because of the same reason as given earlier, its intensity is significantly reduced.

The important message hitherto received by us is that beyond $\eta \geq 4.5$, there occurs some kind of *stabilization* in $\langle R_{ex} \rangle$ irrespective of dopant location. Thus, it goes without saying to conduct a more detailed inspection of this η domain. Driven by this, we have now monitored the $\langle R_{ex} \rangle$ vs r_0 profile, keeping η fixed at 5.0 (Figure 3). Such a study also permits us to explore the

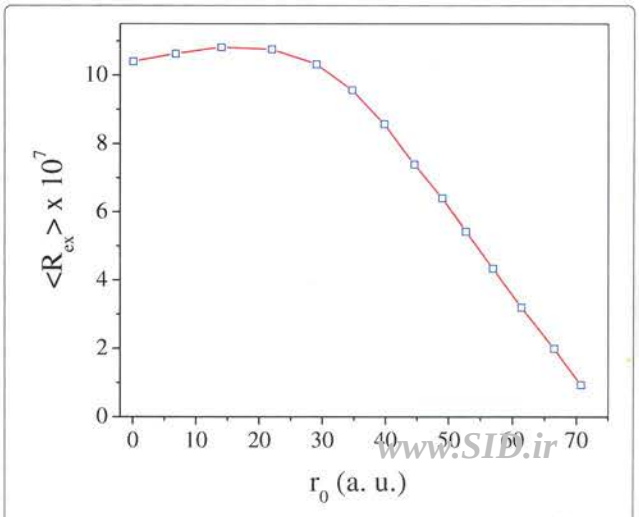

Figure 3 Plot of $\langle R_{ex} \rangle$ vs r_0 at $\eta = 5.0$ with $\gamma_0 = 4.0 \times 10^{-6}$ a.u. and $V_0 = 1.0 \times 10^{-6}$ a.u.

exclusive dependence of the excitation rate on dopant location when the said rate attains considerable stabilization. The plot reveals that after some initial steady value ($r_0 \approx 22.0$ a.u.), the excitation rate decreases monotonically as the dopant is progressively shifted to more and more off-center locations. As we have pointed out earlier (in the context of Figure 1), the decrease in dot-impurity overlap associated with the above dopant shift makes it convenient for the factors that resist excitation to supersede the factors that have the reverse impact. The decrease in the excitation rate becomes the obvious outcome.

Conclusions

The excitation profile of repulsive impurity-doped quantum dots triggered by simultaneous oscillations of the impurity coordinate and impurity spread reveals noteworthy features. The ratio of two oscillations (η) has been found to play a governing role in influencing the excitation rate. We have found a kind of stabilization in the excitation rate when η exceeds some threshold value at all dopant locations. However, before that threshold value, the excitation rates exhibit different trends depending on the dopant coordinate. A critical analysis of the η domain when the excitation rate attains the steady behavior reveals the exclusive role played by the dopant coordinate towards excitation. The analysis evinced maximization and minimization in the excitation rate at some particular dopant coordinate. Whereas the maximization/minimization occurs due to a change in the relative preponderance of various factors that assist or resist excitation, the observed stabilization can be explained by arguing a kind of compromise between the aforesaid factors. The said change in the relative dominance of the responsible factors in turn stems from the interplay between two oscillations. The two oscillations may sometimes reinforce each other, while in other occasions, they can rescind. To be precise, the present investigation reveals that it is the coupled effect of dopant's coordinate and the dopant's spatial spread which ultimately shapes the excitation rate. The results are thus quite interesting and expected to convey important insights in technological applications of quantum dot nanomaterials.

Competing interests

The authors declare that they have no competing interests.

Authors' contributions

SP has carried out mostly the mathematical calculations, whereas MG mostly did the computations and supervised the entire work as a whole. Both authors have read and approved the final manuscript.

Acknowledgements

The authors SP and MG thank D. S. T-F. I. S. T (Govt. of India) and U. G. C.-S. A. P (Govt. of India) for the partial financial support. Thanks are also due to Mr. Nirmal Kr Datta for his cooperation.

Author details

[1]Department of Chemistry, Hetampur Raj High School, Hetampur, Birbhum, West Bengal, 731124, India. [2]Physical Chemistry Section, Department of Chemistry, Visva Bharati University, Santiniketan, Birbhum, West Bengal, 731235, India.

Received: 26 June 2012 Accepted: 9 November 2012
Published: 28 November 2012

References

1. Koenraad, PM, Flatté, ME: Single dopants in semiconductors. Nat. Mater. **10**, 91–100 (2011)
2. Duque, CA, Porras-Montenegro, N, Barticevic, Z, Pacheco, M, Oliveira, LE: Effects of applied magnetic fields and hydrostatic pressure on the optical transitions in self-assembled InAs/GaAs quantum dots. J. Phys.:Condens. Matter. **18**, 1877–1884 (2006)
3. Pacheco, M, Barticevic, Z, Tutor, J: Stark optical transitions in bidimensional arrays of quantum dots. Solid. State Commn. **117**, 667–672 (2001)
4. Karabulut, I, Şafak, H, Tomak, M: Nonlinear optical rectification in asymmetrical semiparabolic quantum wells. Solid. State Commn. **135**, 735–738 (2005)
5. Movilla, JL, Planelles, J: Off-centering of hydrogenic impurities in quantum dots. Phys. Rev. B. **71**, 075319 (2005)
6. Kelly, MJ: Low-Dimensional Semiconductors. Oxford University Press, Oxford (1995)
7. Gülveren, B, Atav, Ü, Sahin, M, Tomak, M: A parabolic quantum dot with N electrons and an impurity. Physica E. **30**, 143–149 (2005)
8. Gülveren, B, Atav, Ü, Tomak, M: Electronic properties of a large quantum dot at a finite temperature. Physica E. **28**, 482–490 (2005)
9. Räsänen, E, Könemann, J, Puska, RJ, Haug, MJ, Nieminen, RM: Impurity effects in quantum dots: toward quantitative modeling. Phys. Rev. B. **70**, 115308 (2004)
10. Aichinger, M, Chin, SA, Krotscheck, E, Räsänen, E: Effects of geometry and impurities on quantum rings in magnetic fields. Phys. Rev. B. **73**, 195310 (2006)
11. Sahin, M, Tomak, M: The self-consistent calculation of a spherical quantum dot: a quantum genetic algorithm study. Physica E. **28**, 247–256 (2005)
12. Baskoutas, S, Paspalakis, E, Terzis, AF: Electronic structure and nonlinear optical rectification in a quantum dot: effects of impurities and external electric field. J. Phys: Cond. Mat. **19**, 395024 (2007)
13. Karabulut, I, Baskoutas, S: Linear and nonlinear optical absorption coefficients and refractive index changes in spherical quantum dots: effects of impurities, electric field, size, and optical intensity. J. Appl. Phys. **103**, 073512 (2008)
14. Nistor, SV, Stefan, M, Nistor, LC, Goovaerts, E, Van Tendeloo, G: Incorporation and localization of substitutional Mn^{2+} ions in cubic ZnS quantum dots. Phys. Rev. B. **81**, 035336 (2010)
15. Nistor, SV, Nistor, LC, Stefan, M, Mateescua, CD, Birjega, R, Solovieva, Nikl: Synthesis and characterization of Mn^{2+} doped ZnS nanocrystals self-assembled in a tight mesoporous structure. Superlattices and Microstructures. **46**, 306–311 (2009)
16. Paspalakis, E, Simserides, Baskoutas, CS, Terzis, AF: Electromagnetically induced population transfer between two quantum well subbands. Physica E. **40**, 1301–1304 (2008)
17. Fountoulakis, A, Terzis, AF, Paspalakis, E: Coherent single-electron transfer in coupled quantum dots. J. Appl. Phys. **074305** (2009)
18. Sung, T, Popovici, G, Prelas, MA, Wilson, RG, Loyalka, SK: Boron diffusion into diamond under electric bias. J. Mater. Res. **12**, 1169–1171 (1997)
19. Murch, GE, Nowick, AS: Diffusion in Crystalline Solids. Academic, Orlando (1984)
20. Sundqvist, PA, Narayan, V, Stafström, S, Willander, M: Self-consistent drift-diffusion model of nanoscale impurity profiles in semiconductor layers, quantum wires, and quantum dots. Phys. Rev. B. **67**, 165330 (2003)
21. Datta, NK, Chatterjee, K, Ghosh, M: Excitations in doped quantum dot driven by linear and non-linear drift of impurity. Solid. State Sci. **13**, 1531–1537 (2011)
22. Datta, NK, Ghosh, M: Excitations in doped quantum dot induced by accelerating impurity center. J. Appl. Phys. **110**, 054314 (2011)
23. Halonen, V, Hyvönen, P, Pietiläinen, P, Chakraborty, T: Effects of scattering centers on the energy spectrum of a quantum dot. Phys. Rev. B. **53**, 6971–6974 (1996)

24. Halonen, V, Pietilinen, P, Chakraborty, T: Optical-absorption spectra of quantum dots and rings with a repulsive scattering centre. Europhys Lett. **33**, 337–382 (1996)
25. Turton, R: The Quantum Dot. A Journey into Future Microelectronics. Oxford University Press, New York (1995)
26. Jacak, L, Hawrylak, P, Wojos, A: Quantum Dots. Springer, Berlin (1998)
27. Adamowski, J, Kwaśniowski, A, Szafran, B: LO-phonon-induced screening of electronelectron interaction in D^- centres and quantum dots. J. Phys:Cond. Mat. **17**, 4489–4500 (2005)
28. Bednarek, S, Szafran, B, Lis, K, Adamowski, J: Modeling of electronic properties of electrostatic quantum dots. Phys. Rev. B. **68**, 155333 (2003)
29. Szafran, B, Bednarek, S, Adamowski, J: Parity symmetry and energy spectrum of excitons in coupled self-assembled quantum dots. Phys. Rev. B. **64**, 125301 (2001)
30. Gharaati, A, Khordad, R: A new confinement potential in spherical quantum dots: modified Gaussian potential. Superlattices and Microstructures. **48**, 276–287 (2010)
31. Gradshteyn, IS, Ryzhik, IM: Tables of Integrals, Series, and Products (corrected and enlarged edition). Academic, New York (1980)
32. Chakraborty, T: Quantum Dots: A Survey of the Properties of Artificial Atoms. Elsevier, Amsterdam (1999)
33. Xie, W: Excited state absorptions of an exciton bound to an ionized donor impurity in quantum dots. Optics Comm. **284**, 5730–5733 (2011)

doi:10.1186/2251-7235-6-42
Cite this article as: Pal and Ghosh: **Influence of periodically propagating impurity and accompanying time variation of impurity spread on excitation profile of doped quantum dots.** *Journal of Theoretical and Applied Physics* 2012 **6**:42.